Topological effects in ring polymers. II. Influence of persistence length

M. Müller,[1,2] J. P. Wittmer,[2,3,*] and M. E. Cates[2]
[1]*Institut für Physik, Johannes-Gutenberg Universität, 55099 Mainz, Germany*
[2]*Department of Physics and Astronomy, University of Edinburgh, King's Building, Mayfield Road, Edinburgh EH9 3JZ, United Kingdom*
[3]*Département de Physique des Matériaux, Université Claude Bernard and CNRS, 69622 Villeurbanne, France*
(Received 3 August 1999)

The interplay of topological constraints and the persistence length of ring polymers in their own melt is investigated by means of dynamical Monte Carlo simulations of a three-dimensional lattice model. We ask if the results are consistent with an asymptotically regime where the rings behave like (compact) *lattice animals* in a self-consistent network of topological constraints imposed by neighboring rings. Tuning the persistence length provides an efficient route to increase the ring overlap required for this mean-field picture to hold: The *effective* Flory exponent for the ring size decreases down to $\nu \lesssim 1/3$ with increasing persistence length. Evidence is provided for the emergence of one additional characteristic length scale $d_t \propto N^0$, only weakly dependent on the persistence length and much larger than the excluded volume screening length ξ. At distances larger than d_t the conformational properties of the rings are governed by the topological interactions; at smaller distances rings and their linear chain counterparts become similar. (At distances smaller than ξ both architectures are identical.) However, the crossover between both limits is intricate and broad, as a detailed discussion of the local fractal dimension (e.g., obtained from the static structure factor) reveals. This is due to various crossover effects which we are unable to separate even for the largest ring size ($N=1024$) presented here. The increased topological interactions also influence the dynamical properties. Mean-square displacements and their distributions depend crucially on the ring overlap, and show evidence of the existence of additional size and time scales. The diffusion constant of the rings goes down from effectively $D_N \propto N^{-1.22}$ for flexible rings with low overlap to $D_N \propto N^{-1.68}$ for strongly overlapping semiflexible rings.

PACS number(s): 61.25.Hq, 61.41.+e, 83.10.Nn, 83.20.Fk

I. INTRODUCTION

Unconcatenated and unknotted rings in their melt are relatively compact [1,2]. This was found in recent computational studies [3–5], and was expected on theoretical grounds [6–9]. Qualitatively the squeezing of the rings was attributed to the topological constraints [see Fig. 1(a)] [10]. This is in line with much older observations showing that dilute rings repel each other much more strongly than their linear chain counterparts due to the entropy loss associated with the unconcatenation constraint, preventing the two rings from threading each other [11]. While the usual excluded volume interaction is screened out at high chain overlap (i.e., if the ring size R is larger than the size ξ of the excluded volume blob) [12,13], topological interactions are expected to dominate the conformational properties if the number of overlapping rings $p \approx R^3\phi/N$ (N being the chain mass, ϕ the monomer density) becomes high enough.

In a simple Flory-like argument, Cates and Deutsch (CD) [6] argued that the number of degrees of freedom lost for a typical ring due to its topological interactions with neighboring rings increases as p^α, where α is an unknown exponent. This free energy term, which favors decreasing ring size, has to be balanced by the entropy penalty for squashing a ring. To be specific, this penalty was assumed to be the same as for a Gaussian chain. Adding these contributions and minimizing over $R \propto N^\nu$ yields the Flory exponent $\nu=(\alpha+1)/(3\alpha+2)$. The simplest possible estimate for α is to say that roughly one degree of freedom is lost for each of the p neighbors which the ring is prevented from threading, i.e., $\alpha=1$ and hence $\nu=2/5$. This is very close to the value $\nu \approx 0.39$ found by us in our previous study [4]. Note that the overlap number $p \propto N^{1/5}$ increases extremely weakly, and that the only intrinsic length scale in the CD picture is the ring size R itself (possibly renormalized in terms of excluded volume blobs of size ξ). Again this was found to be in qualitatively good agreement with the simulations reported in our first paper [4]. From the CD picture one expects a similar density crossover scaling for rings as for linear chains: The ring size $R(\phi)$, reduced by the ring size R_0 of the dilute reference ring, should scale with ϕ/ϕ^*, where $\phi^* \approx N/R_0^3$ is the crossover density. Having focused in Ref. [4] on *flexible* rings at one fixed density, we were unable to verify this implicit scaling assumption of the CD picture.

A different picture comes from the extensive studies on (isolated) ring polymers in gels [see Fig. 1(b)], often modeled by so-called *lattice animals* (LA's), depicted in Fig. 1(c) [6,7,9]. If the ring size R becomes larger than the typical distance d_t between the fixed topological obstacles (represented as squares in the figure) the rings are forced to retrace their paths and the fractal dimension $d_f=1/\nu$ becomes that of a strongly branched object. The question is now if it is also possible to use this well-understood model via a standard mean-field argument for strongly overlapping systems of rings in their own melt. Are the surrounding rings able to generate (in a self-consistent manner) a fixed mesh of topological obstacles around a reference ring? If so, is $d_t \propto R$—in

*Author to whom correspondence should be addressed.

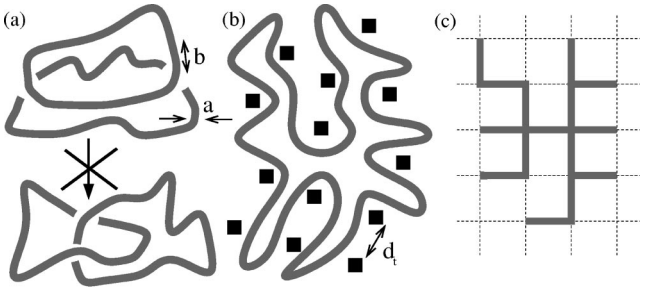

FIG. 1. Sketch of topological constraints and their effects. (a) The top chains present allowed conformations of unknotted and (more importantly) unconcatenated rings. The rings cannot turn into knotted configurations (not shown) or the concatenated configurations shown on the bottom. It is this nonlinkage constraint which tends to *squeeze* a ring in semidilute solutions and melts. The interplay between the topological constraint and the effective bond length b (in contrast to the monomer size a) is studied here. (b) One ring in a network of *fixed* topological constraints or obstacles (squares) imposing a strongly entangled and compact conformation. (c) An equivalent lattice animal (LA): In the high overlap limit rings are expected to behave effectively like LA's. This is mean-field picture for a reference ring within a self-consistent topological network imposed by the surrounding rings.

FIG. 2. Configurational snapshots of rings of mass $N=256$: dilute flexible ring in the middle, flexible ($\sigma=0$) ring in the melt ($\phi=0.5$) on the left, and corresponding semiflexible ($\sigma=3$) coil on the right. The overlap has increased by factor 3 between the flexible and semiflexible chains in the melt. To obtain a similar effect by increasing the chain mass we would have to increase N by at least two orders of magnitude.

which case the LA and CD pictures would be indistinguishable from the scaling point of view—or does it introduce an additional ring length independent scale? In the latter case, obviously, the above mentioned density crossover scaling would not work. (However, one can strictly only expect this LA picture to hold in the high entanglement limit.) In any case, there is a catch: While increasing $p \propto b^3 N^{3\nu-1}$, b being the persistence length, the effective exponent $\nu(p)$ is supposed to drop down to 1/3 (and even down to $\nu=1/4$ for an ideal Gaussian LA within an intermediate range of ring sizes N) [7]. Hence the LA picture might not be self-consistent, as already stressed in Ref. [6]. It is crucially the prefactor b^3 (and not the inefficient $N^{3\nu(p)-1}$) which allows the simulator to control the overlap. (This assumes that the persistence length only weakly affects the hypothetical length d_t which has to be checked *a posteriori*.)

This is the route we have taken in this study to test the scaling predictions (rather than the variation in density ϕ which we plan to investigate in a subsequent study [14]). Indeed, the persistence length b turns out to be a very efficient way to vary the overlap number p (additional computational overhead and reduced diffusion constants taken into account) compared to the ring mass (which we have however increased from $N=512$ to 1024). This allows us to more severely put a test on the scaling predictions of the CD scenario than we were able to do in our previous study [4]. In contrast to that work, the evidence presented here shows the emergence of (at least) one further length scale alongside R which we identify with d_t. Tentatively, our data are consistent with a broad crossover toward the LA picture in the limit of high chain overlap which is attained by increasing b so that the chains become more extended (though more compact in the scaling sense of smaller ν). A typical semiflexible coil at higher overlap is presented in Fig. 2 on the right.

Of course, the CD and LA pictures are not necessarily contradictory in that they might provide useful heuristic descriptions in different overlap limits. In the computationally important regime (depending on b) where the rings expel successfully neighboring chains and form relatively dense coils, the mean-field assumption of the LA approach has to break down. A typical chain for low overlap is shown Fig. 2 on the left. The CD picture is *a priori* a good candidate to describe this regime where overlap p and topological interactions are weak. A possible choice for the unknown CD exponent in this regime is the limiting case $\alpha \to 0$ and, hence, $\nu \approx 1/2$, i.e., the topological constraints mainly contribute *logarithmic* corrections to a closed [10] Gaussian chains of blobs. Evidence for this (justifying *a posteriori* the squeezing term used by CD) is presented below.

Our paper is arranged as follows: In Sec. II we give a short synopsis of the model and the simulation technique used. To understand the special effects linked to the unconcatenation constraint, we need reference date at the same chain and persistence length to compare with. This is provided in Sec. III, where we review some properties of dilute semiflexible ring polymers. In Sec. IV, we investigate the statistics of ring polymers in their melt as a function of the stiffness, comparing them with dilute rings and dense linear chains from Refs. [15,16]. (Note that in most figures we compare features discussed subsequently in Secs. III and IV.) Possible scaling scenarios are discussed and a detailed analysis of the local fractal dimension is presented. Section V briefly presents our first results on the dynamics of semiflexible ring polymers. We conclude with a summary of our results.

TABLE I. Persistence length dependent properties for dilute ($\phi=0$) rings and linear chains: Mean cosine of the bond-bond angle $\langle\cos(\Theta)\rangle$, mean bond length l, effective bond length of linear chain b_e^L and rings b_e^R, acceptance rate A, and the diffusion constant ND_N. These values characterize the asymptotic behavior of long linear chains as well as rings.

σ	$\langle\cos(\Theta)\rangle$	l	b_e^L	b_e^R	A	ND_N
0	−0.193	2.736	3	1.55	0.254	0.032
1	−0.394	2.724	3.32	1.73	0.224	0.026
2	−0.554	2.706	3.94	1.89	0.193	0.021
3	−0.668	2.703	4.24	2.24	0.165	0.019

TABLE II. Persistence length dependent properties for rings and linear chains at high volume fraction $\phi=0.5$: Mean cosine of the bond-bond angle $\langle\cos(\Theta)\rangle$, mean bond length l, effective bond length b_e^L for linear chains, acceptance rate A, and differential Flory exponent ν_{eff} fitted over the four largest chains available (see Fig. 3).

σ	$\langle\cos(\Theta)\rangle$	l	b_e^L	A	ν_{eff}
0	−0.106	2.632	3.2	0.1529	0.41
1	−0.348	2.614	3.7	0.1329	0.39
2	−0.544	2.602	4.5	0.1136	0.36
3	−0.676	2.593	5.3	0.0983	0.33

II. ALGORITHM AND PARAMETERS

As in our previous study we investigate the properties of unknotted and unconcatenated rings in the framework of the bond fluctuation model (BFM) [17]. Many static and dynamic properties of linear chains are known for this computationally efficient, coarse grained lattice model. A small number of chemical repeat units is mapped onto a lattice monomer such that the relevant characteristics of polymers—excluded volume and connectivity—are retained. Each monomer blocks a unit cell of the three-dimensional cubic lattice from further occupancy. Adjacent monomers along a polymer are connected via one of 108 allowed bond vectors of lengths 2, $\sqrt{5}$, $\sqrt{6}$, 3, and $\sqrt{10}$. Here and in the following all spatial distances are measured in units of the lattice spacing. This set of bonds allows for 87 different bond angles and, hence, results in a good approximation to chains in continuous space. The bond vectors are chosen such that the local excluded volume interactions prevent the rings from crossing each other during their motion. This conservation of the topology ensures that the rings remain neither knotted with themselves nor concatenated with one another during the course of the simulation. We evolve the ring conformations via random local monomer displacements.

As explained in the Sec. I, a crucial parameter is the overlap number p, which increases only very weakly with N, but much more strongly with the persistence length. In order to tune the persistence length, we impose a simple intramolecular potential which favors straight bond angles: $E(\Theta)=\sigma\cos(\Theta)$. Here Θ denotes the complementary angle between two successive bonds, and σ the dimensionless energy scale (setting $k_BT=1$). This potential has been used and investigated in various studies on linear polymer chains at filling fraction $\phi=0.5$ of occupied lattice sites [16,19]. This is of importance because it is reasonable to assume that on short length scales (for long enough chains) neither ring closure nor topological constraints are pertinent. This statement will be corroborated later in Sec. IV, when we discuss the local ring structure (Fig. 6). Note for now that other local quantities like the mean bond length l, $\langle\cos(\Theta)\rangle$ (i.e., the mean stiffness energy per monomer) or the acceptance rate A are identical for rings and their linear counterparts. Hence one expects to find the same local rigidity $b(\sigma)$ for rings as for linear chains, where $b=b_e^L$ is easily obtained from the mean-square end-to-end vector $\langle R_e^2\rangle$ and the known Flory exponent of linear chains. See Tables I and II for the dilute ($\phi=0$) and dense limits ($\phi=0.5$), respectively. The systems containing dilute rings and linear chains have been simulated for reasons of comparison. Not surprisingly the quantities featured in Tables I and II depend somewhat on the volume fraction [15,16]. Note that at the density $\phi=0.5$ of occupied lattice sites, many static and dynamic features of *molten* linear polymer materials are reproduced by the BFM. For example, the single chain conformations obey Gaussian statistics down to the screening length $\xi(\sigma=0)\approx 6$ of the excluded volume interaction obtained by the static structure factor [15].

We have restricted ourselves to values $\sigma\leqslant 3$, because we found tentative evidence for the onset of a nematic order at values $\sigma\geqslant 4$. Due to the lower conformational entropy, rings tend to order nematically at lower stiffnesses than linear molecules. (For linear chains an isotropic to nematic transition is found close to $\sigma\approx 6$ [16].) Moreover, increasing the stiffness also decreases the number of statistically independent segments, and we want to keep finite N effects low, even for small ring lengths.

The algorithm described above has been implemented on a massively parallel Cray T3E computer [18]. Using a two-dimensional geometric decomposition of the simulation grid of linear extension $L=128$, we employ 64 T3E processors. The simulations involve about 40 000 hours of single processor CPU time.

As shown in Table III, this allows us to investigate ring systems with 131 072 monomers and chain masses up to $N=1024$. The data for flexible rings have been used as starting configurations for simulations at higher persistence length. In most cases rings diffused at least a spatial distance of their radius of gyration before any conformational data were collected. The simulation runs were extended up to five times the relaxation time for sampling the ring conformations. Note that we could not meet this stringent criterion for the semiflexible ($\sigma>0$) systems at our largest mass $N=1024$. The resulting data appear to be time independent, and we presume them to be equilibrated, but they have not diffused over a radius of gyration. These three data points ($\sigma=1$, 2, and 3) have to be taken with care.

As can be deduced from Table III, a relatively small increase in persistence length is a very effective way to increase the overlap number $p\propto R_e^3/N$. To give some numbers, increasing the stiffness parameter σ from 0 to 3 amounts to increasing p by a factor 3 for $N=256$ (seen in Fig. 2) and by a factor 5 for $N=512$. To achieve a similar effect by tuning the contour length requires an increase by two (respectively three) orders of magnitude [20].

TABLE III. Ring radius of gyration R_g, diameter R_e, and (reduced) diffusion constant ND_N10^3 for different ring sizes N and stiffnesses σ at $\phi=0.5$.

	$\sigma=0$			$\sigma=1$		$\sigma=2$		$\sigma=3$		
N	$\langle R_g^2\rangle$	$\langle R_e^2\rangle$	ND_N10^3	$\langle R_g^2\rangle$	$\langle R_e^2\rangle$	$\langle R_g^2\rangle$	$\langle R_e^2\rangle$	$\langle R_g^2\rangle$	$\langle R_e^2\rangle$	ND_N10^3
16	12.9	42.3	5.87	16.4	54.1	21.3	73.9	26.2	95.3	1.94
32	25.7	80.6	5.18	32.9	102	44.7	141	60.2	198	1.23
64	49.3	150	4.21	63	189	84.5	251	117	353	0.77
128	92.2	275	3.65	115	337	150	430	203	579	0.4
256	169	492	3.23	204	581	250	700	330	910	0.38
512	297	856		343	978	420	1157	490	1315	
1024	514	1474		539	1680	620	1784	710	2140	

III. DILUTE RINGS REVISITED

As a reference for the subsequent section on strongly overlapping rings (where the unconcatenation constraint matters) we briefly revisit some properties of flexible and *semiflexible* dilute rings and their linear counterparts. Basically, the remaining unknottedness constraint and the requirement of ring closure [10] do not matter: Dilute rings behave broadly like linear chains.

The simplest quantity to characterize the chain structure as a function of the stiffness parameter σ is the overall chain size versus chain length N. The size of the rings is measured first with the usual mean-square radius of gyration $\langle R_g^2\rangle$. As a second measure, we sample the mean-square distance $\langle R_n^2\rangle=\langle(\vec{R}_i-\vec{R}_{i+n})^2\rangle$ (averaged over all monomers i) between pairs of monomers that are n monomers apart along the contour. In particular, for rings, we define the mean-square ring diameter $\langle R_e^2\rangle=\langle R_n^2\rangle|_{n=N/2}$. (For the linear chains $\langle R_e^2\rangle=\langle R_n^2\rangle|_{n=N}$ denotes the usual mean-square end-to-end distance.) In Fig. 3 the diameter $R_e=\langle R_e^2\rangle^{1/2}$ for flexible and semiflexible dilute rings is plotted versus N. Not included are the linear counterparts of same N and σ. (But see Fig. 4.) The data are well fitted for all the persistence lengths considered by $R_e=b_eN^\nu$ with the classical Flory exponent $\nu=\nu_0\approx 3/5$ [21]. The effective bond length b_e encodes the persistence length effect. It is tabulated for linear chains (L) and rings (R) in Table I. Similar fits have also been performed for the radius of gyration. We find, independent of chain size and persistence length, the following relations: $b_e^L/b_e^R\approx 1.89$, $b_g^L/b_e^L\approx\sqrt{6}$, and $b_e^R/b_g^R\approx 1.79$. Note that in fitting we have disregarded the three smallest masses $N=16$, 32, and 64 to minimize finite size effects. We have checked for (the remaining) finite size effects (not shown): The (negative) curvature in the data points is surprisingly weak and *similar* for linear chains and rings. It is slightly stronger for the radius of gyration than for the diameter which probes larger distances. While we cannot rule out that the asymptotic exponents of the ring chains are slightly different from their linear counterparts, for all practical purposes of relevance here we may conclude that neither the ring closure nor the non-self-knottedness constraint are pertinent.

We are now in the position to rescale the effects of the persistence length for both linear chains and rings by estimating for the linear chain the number g_k of correlated monomers along the chain and the associated Kuhn length $k=lg_k$ (l being the measured mean length of the BFM bond). Rewriting $R_e=b_eN^\nu=k(N/g_k)^\nu$ yields $g_k=(b_e/l)^{1/(1-\nu)}$ and $k=l(b_e/l)^{1/(1-\nu)}$. Obviously this scaling-based definition of k and g_k is arbitrary to within prefactors of order 1. The proposed rescaling works successfully for dilute linear chains and rings, as shown in Fig. 4. Here we have plotted the reduced diameters $u=R_e/k$ versus the number of statistical segments $v=N/g_k$. A similar figure was obtained for the radius of gyration (not shown). Note that only a part of the linear chain configurations used to characterize the stiffness effects for dilute systems are included in the figure.

In Fig. 5 we show the bond-bond correlation function $\langle\vec{e}_i\cdot\vec{e}_{i+n}\rangle$, where $\vec{e}_i$ denotes one of the bond vectors of monomer i (say the ''right'' one in a given list). Only values for rings are included (the values for linear chains being identical for long enough chains). As it should, the bond-bond correlation functions for different persistence lengths collapse onto a single scaling curve, when plotted versus

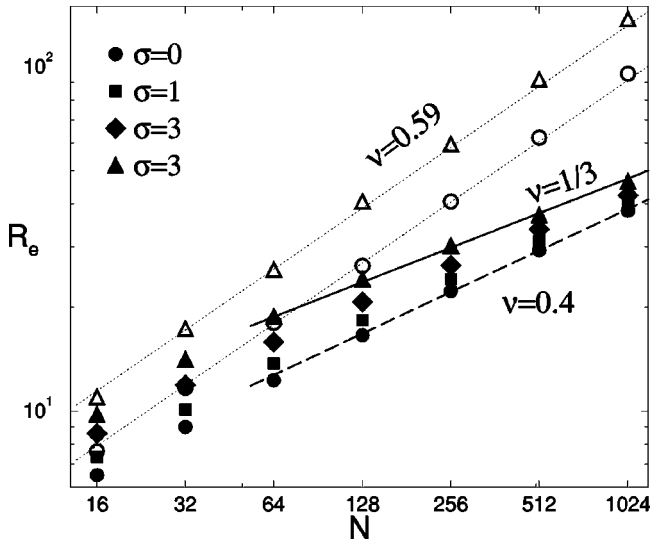

FIG. 3. Diameter R_e vs chain length N for different σ for dilute (open symbols) and dense (full symbols) rings. The dilute rings are characterized by the same Flory exponent $\nu=\nu_0\approx 0.59$ as their linear counterparts (not shown). For large enough chains this is independent of σ. For the dense chains the effective fractal dimension $d_f=1/\nu$ becomes much larger, depending strongly on the chain rigidity: flexible chains ($\sigma=0$) compare well with $\nu=0.4$ (dashed line), semiflexible chains ($\sigma=3$) with $\nu=1/3$ (solid line).

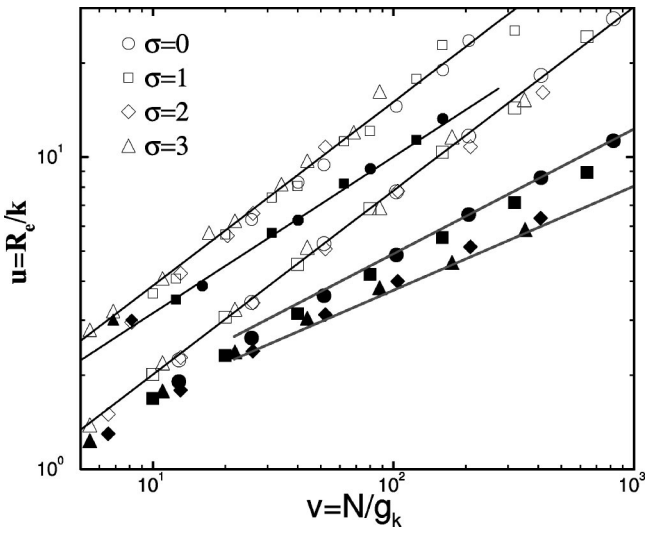

FIG. 4. Reduced diameter $u=R_e/k$ vs reduced chain mass $v=N/g_k$ for dilute ($\phi=0$, open symbols) and dense ($\phi=0.5$, full symbols) linear chains (top two lines) and rings (bottom). The chain flexibility σ changes as indicated in the figure. The lines indicate (effective) exponents (from top to bottom) $\nu=0.59$ for dilute linear chains, $\nu=0.5$ for dense linear chains, $\nu=0.59$ for dilute rings, $\nu=0.4$ for dense, flexible ($\sigma=0$) rings, and $\nu=1/3$ for semiflexible ($\sigma=3$) rings in the melt. Note that the dense rings do not collapse on one master curve as their linear counterparts.

n/g_k (not shown). Note that this scaling and the (supposed) exponential decay is sometimes preferred to define the number of correlated monomers g_k and the persistence length k rather than our definition based on the measured effective bond length b and the well-known (and for rings confirmed) Flory exponent. However, the correlation function for dilute chains (both linear and rings) certainly does *not* decrease as a pure exponential (not shown). This is due to (nonuniversal) short range packing effects and (more importantly) to long range excluded volume correlations. In addition to this we prefer our method for statistical reasons.

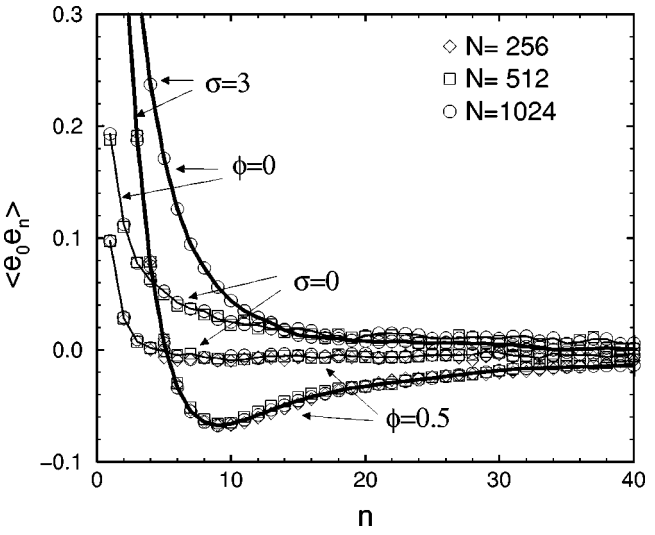

FIG. 5. Bond-bond correlation function $\langle e_0 e_n\rangle$ for dilute ($\phi=0$) and molten ($\phi=0.5$) rings for $\sigma=0$ (connected by thin lines) and $\sigma=3$ (connected by fat lines) for various chain masses as indicated in the figure. At high chain overlap (high density and rigidity) we find a pronounced negative dip in the correlation function.

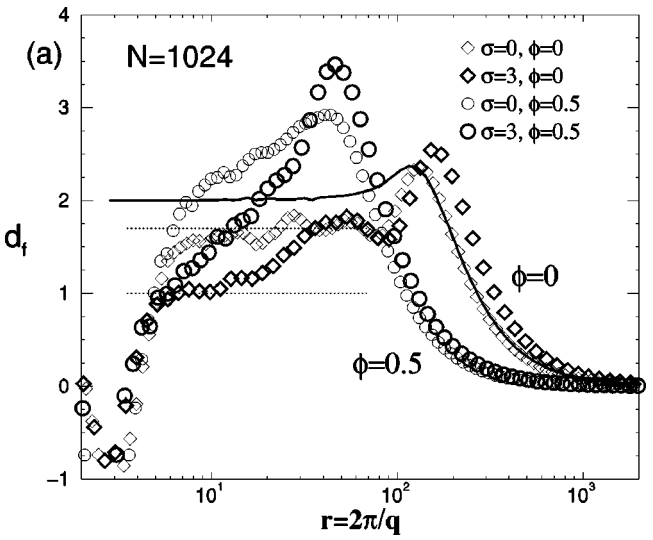

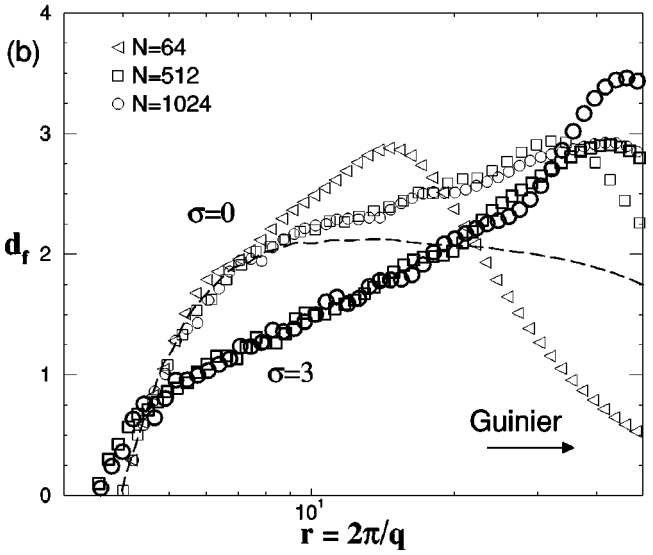

FIG. 6. Differential fractal dimension $d_f(q)=-d\log(S(q))/d\log(q)$ vs $r=2\pi/q$. (a) Dilute and molten rings of mass $N=1024$. The line indicates an ideal Gaussian ring of same radius of gyration as a flexible and dilute ring. (b) Rings in their melt ($\phi=0.5$). The dotted line is a comparison with linear chains ($N=256,\phi=0.5$). Within the first blob [$r<\xi(\sigma)$], linear chains and rings behave identically.

Additional information about the local structure of the flexible and semiflexible rings comes from the structure factor $S(q)$ which is of direct experimental relevance. The slopes of the structure factor in log-log coordinates define the differential fractal dimension $d_f(q)=-d\log(S(q))/d\log(q)$. The general shape of $S(q)$ was discussed in Ref. [4]. Here we present only $d_f(q)$ which contains all the information. It is equivalent in the limit of long chains ($q\to 0$, $qR_g\gg 1$) to the inverse of the Flory exponent ν. Figure 6(a) shows $d_f(q)$ for dilute rings (thin symbols) of mass $N=1024$ plotted versus $r=2\pi/q$. For large distances the rings are well described by the classical Guinier expansion $S(q)\approx N(1-(R_g q)^2/3)$ (not shown); hence $d_f(qR_g\to 0)\to 0$. For small distances $r\approx l$ one finds the usual spurious Bragg peak of the structure factor [4] due to

local packing effects giving rise to negative d_f-values. We note a weak σ dependence due to BFM related lattice effects: A slightly different set of bond vectors is preferred. This is in line with the fact that also the mean bond vector varies weakly with persistence length, as shown in Table I. In between both limits we find a broad plateau for the flexible rings with $d_f = 1/\nu_0 \approx 1.7$ (upper horizontal line) due to the excluded volume interactions. Semiflexible rings show, as expected from linear chains, a shoulder at about $d_f = 1$ (upper horizontal line) due to the local rigidity of the rings. Note that the curves for linear dilute chains (not included) are very similar. The only qualitative difference is the ''hump'' between the plateau and the Guinier regime. This is due partially to the ring closure, as one can easily see by calculating the static structure factor for a Gaussian ring (solid line).

IV. CONFORMATIONAL PROPERTIES OF DENSE RINGS

A. Compact, but strongly overlapping rings

While dilute rings essentially behave like their linear counterparts, this becomes very different for unconcatenated rings in the melt. This is shown in the dramatic decrease of the chain size of rings (full symbols) in Fig. 3 as compared with dilute reference rings (open symbols). Certainly, linear chain sizes also decrease with increasing density due to the screening of the excluded volume correlations [12,15], but to nowhere near this extent, as Fig. 4 illustrates. Moreover, the slopes of R_e versus $v = N/g_k$ decrease strongly with persistence length (see Table II.) For flexible rings ($\sigma = 0$) the data points (for $N = 128$–1024) are fitted by an (effective) exponent $\nu = 0.4$. For our stiffest rings we observe $\nu(\sigma = 3) \approx 1/3$. This last result is indeed consistent with the compact LA scaling behavior predicted for rings at high enough overlap p.

These results are also in agreement with the density distribution of a ring around its center of mass, shown for rings in Fig. 7. We see that for flexible rings (main figure) the overlap p must be very small; nearly all monomers from neighboring rings are expelled. From the Flory exponent $\nu \approx 0.4$ measured above one expects the density inside the ring to decrease as $\rho \sim N^{-0.2}$. This is confirmed. In the inset we present the corresponding plot for semiflexible rings ($\sigma = 3$). Since the effective Flory exponent is $\nu = 1/3$ we expect the density inside the ring to be independent of the ring size. The ring length independence of the density is observed for $N \gtrsim 128$ for $\sigma = 2$ (not shown) and $N \gtrsim 64$ for $\sigma = 3$. This supports the idea that the LA regime is reached earlier for stiffer rings. Though rings in this regime show compact scaling ($\nu \approx 1/3$), the asymptotically constant density ρ is fairly small. Thus the density of *other* rings in the correlation hole of a given ring is *larger* for stiff than for flexible rings (Fig. 7). This holds for the ring sizes studied; it does not exclude similar strong overlap behavior for flexible, but much larger, rings.

B. First evidence for additional length scale

We have to stress, however, that the above exponents are only *effective* exponents. The curves are strongly (negatively) curved, as one can easily visualize by plotting $R/N^{1/3}$ versus N (not shown). Alternatively, one can characterize this curvature via the differential Flory exponent $\nu(N)$ defined from the increase between chain length N and $2N$ [4]. This reveals (not shown) that $\nu(N)$ decreases continuously from $\nu \approx 1/2$, i.e., nearly Gaussian behavior, for smaller rings down to the slopes indicated in Fig. 3 for the largest masses we were able to simulate. In our previous study [4] we have attributed the observed curvature to classical finite-size effects which also appear for linear chains. That is, we have not attributed them to topological effects, but excluded volume interactions visible due to the finite number of blobs. If one admits this as the *only* physical origin of the curvature (excluding, e.g., additional length scales) it is indeed reasonable to attempt to obtain the asymptotic exponent by classical finite-size extrapolation method. In this method, the local slope $\nu(N)$ (obtained from the diameter and the radius of gyration) is plotted versus the reduced blob size ξ/R, where R is itself given in a self-consistent manner by the asymptotic behavior. This works generally well for linear polymers. Proceeding along these lines we obtained an asymptotic exponent of $\nu \approx 0.4$ (which we now obtain directly after including $N = 1024$). This value happened to coincide with the CD picture ($\alpha = 1$ [6]), which made us perhaps more confident than we should have been (in Ref. [4]) of having characterized the asymptotic behavior.

The excluded volume effects (and their screening) do certainly contribute to the general crossover scenario. This is shown below when we discuss the structure factor (Fig. 6). But a danger remains that we may have missed additional physics, in the form of an additional length scale (not included in the simple CD picture), which controls the behavior of molten rings.

Thus one of the key claims made in Ref. [4] was that the only relevant length scale in dense rings is the chain size

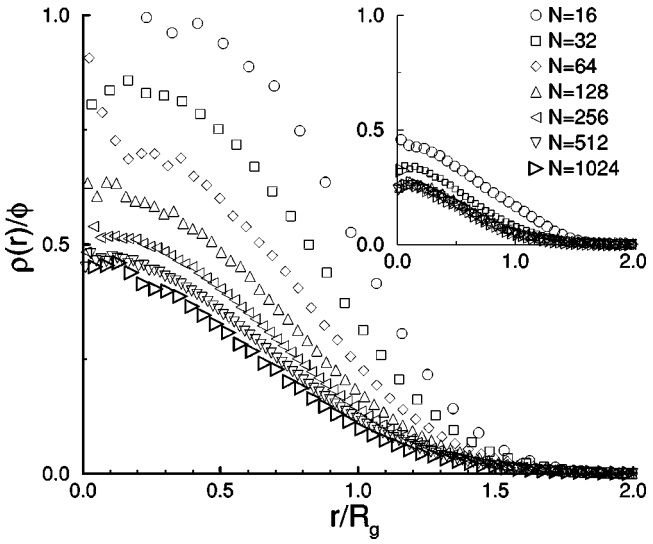

FIG. 7. Single chain density distribution with respect to its center of mass for dense systems $\phi = 0.5$ with flexible rings ($\sigma = 0$) vs reduced distance r/R_g. The density at the center of the coil decreases ($R_g^3/N \propto N^{-0.2}$, in agreement with the effective exponent from Fig. 3), but always remains larger than 0.4ϕ. The inset presents the same for semiflexible rings ($\sigma = 3$); the (rescaled) distribution density becomes chain length independent for $N \leqslant 64$ (the density at the center $\approx 0.25\phi$).

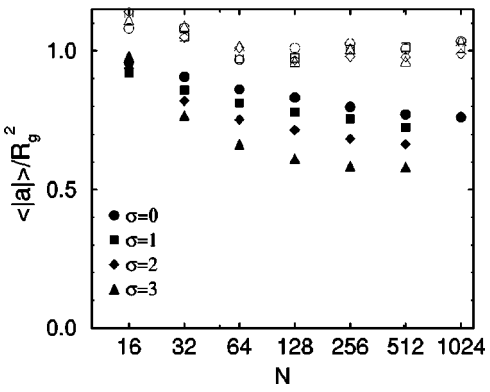

FIG. 8. Reduced area $\langle|a|\rangle/\langle R_g^2\rangle$ vs N for dilute rings (open symbols) and molten rings (full symbols) for different σ. Note the logarithmic, but systematic, correction to the scaling for the latter.

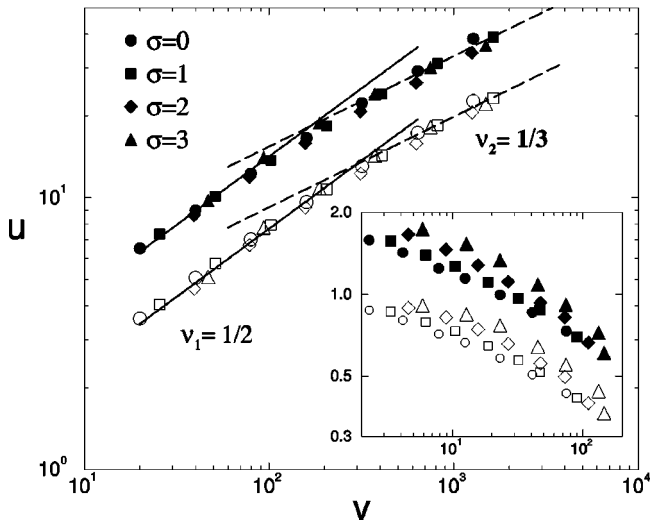

FIG. 9. Two scaling attempts for diameter (full symbols) and radius of gyration (empty symbols) at different flexibilities as indicated in the figure. In the inset we try the traditional scaling $u=R/R_0$ vs $v=\phi/\phi^*\approx R_0^3\phi/N$. The poor scaling evidences additional length scales. In the main figure we explore the possibility of a length scale d_t assumed to be independent of both mass N and persistence length σ. We plot $u=R/d_t$ vs $v=N/g_t$, where we set arbitrarily $d_t=1$ and fix $g_t/g_k=(d_t/k)^2$ self-consistently with the observed effective Gaussian behavior at short distances. All data points collapse. The slopes indicate Gaussian behavior for $R<d_t$ ($\nu_1=0.5$: solid line) behavior for $R<d_t$, and compact LA ($\nu_2=1/3$: dashed line) behavior for larger distances.

itself. This was shown in various scaling plots, e.g., of the reduced mean ring ''area'' $\langle|a|\rangle/\langle R_g^2\rangle=$const. The area a is defined as a signed quantity (the component in that direction of the vector area of a ring) that vanishes for any configuration in which the ring exactly retraces its own steps. Qualitatively, one expects that a ring which is only very weakly threaded by the surrounding rings has a very small area. This should hold in particular while we approach the LA limit. The reduced area $\langle|a|\rangle/\langle R_g^2\rangle$ has been (log-linear) plotted in Fig. 8 versus ring mass N for dilute rings (empty symbols) and rings in the melt (full symbols) of different flexibility. For (long enough) *dilute* rings the ratio is indeed chain length (and persistence length) independent. For the dense limit, however, we now find evidence of (logarithmic) corrections to the expected CD scaling (plateau). The reduced area decreases systematically as a function of mass—this is in contrast to what was deduced from a (linear-linear) plot in Ref. [4]. Note that the ratio also decreases with respect to σ: stiffer rings are likely to be less threaded by other rings. This is consistent with the LA picture, where stiffer (and hence larger) rings are forced to retrace their own steps in a network of fixed obstacles.

C. Failure of classical scaling analysis without additional length scale

More stringent tests for the CD picture are posed by the following two scaling analyses, which try to allow for a varying persistence length under the assumption of no new additional length scale for topological interactions. They are presented in Fig. 4 and in the inset of Fig. 9.

In the first we replot the reduced ring size $u=R_e/k$ versus the number of statistical units $v=N/g_k$ as we did in Sec. III for dilute rings. The values of k and g_k used in Fig. 4 for the dense linear chains and rings are the same as for the dilute systems [22]. The difference from the behavior of linear chains is striking: The ring data for different σ lines *diverge*, while the linear chain data clearly collapse (on the expected slope $\nu=0.5$). This is a physically unsound result; flexibility-dependent universality classes for rings are difficult to accept.

The second scaling test is the ''classic'' $u=R(\sigma,\phi=0.5)/R_0$ versus $v=\phi/\phi^*\approx N/R_0^3$ mentioned in Sec. I [12]. This is shown in the inset of Fig. 9. Both the ring diameter (full symbols) and radius of gyration (empty symbols) at $\phi=0.5$ have been included. As reference chain size R_0 we used the measured radius of gyration for a dilute ring of given σ. Again, the scaling attempt fails to account for data of more than one chain stiffness.

For the moment we may conclude that there is clear evidence of one or more additional length scales. At this point, we still do not know how this hypothetical length scale d_t depends on ring and persistence lengths, nor do we know what physics it represents: however, since it arises for rings and not for linear chains, we can presume a topological origin.

D. Evidence for a chain length independent length d_t

Another striking effect which we are able to see due to the persistence length variation is shown in Fig. 5 for the bond-bond correlation function of dense rings. As before, for dilute chains this correlation function becomes chain length independent for the large masses indicated in the figure. For flexible rings the correlation function drops down slightly below zero within three monomers and approaches then zero from below. When the persistence length is increased a most remarkable negative correlation becomes visible, indicating that the polymer is likely to fold back after ten monomers for ($\sigma=3$) [23]. Needless to say, the correlation function for dilute rings does not show anything faintly similar. The position and depth of this anticorrelation dip increase with σ. We stress that the position and shape of the dip are chain length independent. If this effect has something to do with

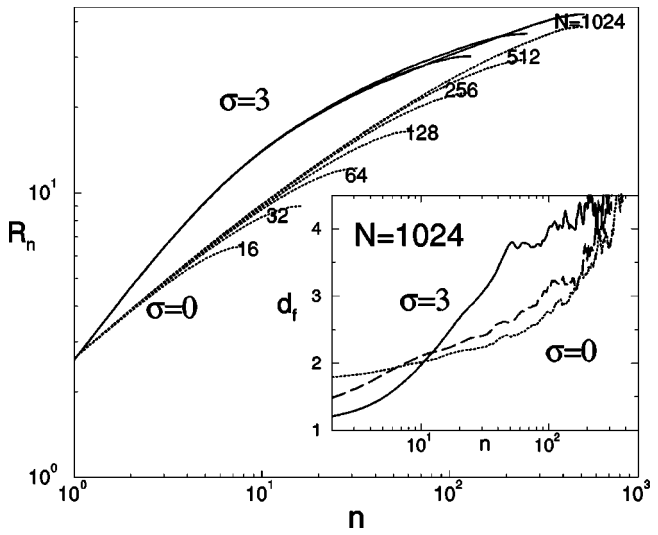

FIG. 10. Distance R_n between a chain contour of length n for $\phi=0.5$. Main figure: Flexible and semiflexible ($\sigma=3$) chains of various chain length N as indicated in the figure. Inset: Differential fractal dimension $d_f(n)=1/\nu(n)$ for $N=1024$ and $\sigma=0$ (dotted line), $\sigma=1$ (dashed line), and $\sigma=3$ (solid line).

the additional length scale d_t mentioned above, as we believe, this is a piece of evidence for its chain length independence.

E. A scaling scenario

This observation forms the basis for the next scaling proposal attempted in Fig. 9. We assume here that there is one additional, mass independent, length scale d_t. Hence the associated number g_t of monomers between the topological obstacles is also mass independent, but depends on the local conformational properties. These are complicated, as will be revealed below (see Figs. 6 and 10). However, as we have observed above (Fig. 3), short rings are reasonably approximated by Gaussian statistics and we may write $g_t = g_k(d_t/k)^{1/\nu_1}$, where ν_1 is some effective exponent close to 1/2 characterizing the (messy) statistics at distances $k \ll r \ll d_t$. We want to plot $u=R/d_t$ versus N/g_t, where R denotes either the diameter (full symbols) or the radius of gyration (empty symbols). We still need to fix the persistence length dependence of d_t. For simplicity, we suppose that d_t is only weakly affected by σ, and arbitrarily set $d_t=1$, i.e., we neglect any stiffness dependence of d_t itself. Hence $g_t \propto 1/g_k$ and $v=Ng_k$. This assumes that the effect of σ is to increase R/d_t (allowing the asymptotic regime to be accessed for smaller N) by increasing R at (nearly) constant d_t. This idea is very much the opposite of what we tried in Fig. 4 where we had $v=N/g_k$, and stiffer chains with fewer statistical units were considered as being effectively ''shorter.'' As shown in Fig. 9, this simple proposal is successful, although a weak dependence of d_t on σ cannot be ruled out. Moreover, it is self-consistent: The local statistics is indeed well described by the Gaussian behavior $\nu_1 \approx 1/2$. This might be interpreted as the $\alpha \to 0$ limit of the CD proposal. The data collapse over two orders of magnitude in v justifies *a posteriori* the neglect of a stiffness dependence of d_t. At large distances data points for *different* persistence lengths fall together on one slope of $\nu_2=1/3$, which is consistent with the LA picture. Note the later crossover of the radius of gyration onto the ν_2 slope. This might be related to the fact that R_g probes smaller distances.

The above proposal may in principle be generalized to incorporate excluded volume effects on intermediate scales $k \ll r \ll \xi$ where the statistics is governed by the exponent $\nu_0=0.59$ for dilute rings. Note that the strong dependence of the excluded volume screening length ξ on the persistence length is checked by the small difference between ν_0 and ν_1. (We plan to consider this problem in a subsequent study on density effects [14].) This offers an effective simplification for the molten chains ($\phi=0.5$) of interest in this study: Both length scales ξ and k are of same order, and we are not able to separate the effects in any case, as we are going to show now.

F. Local conformational properties: Structure factor

So far we have considered mainly global properties like the ring diameter R_e or the ring area. We wish now to characterize the *local* conformational properties by measuring the single chain structure factor $S(q)$ and the mean-square length $\langle R_n^2 \rangle$, both introduced in Sec. III, and the differential fractal dimensions $d_f(q)$ associated with both quantities. We will first consider the fractal dimension obtained from $S(q)$ as presented in Fig. 6, and then compare this in Sec. IV F below) with d_f obtained from $\langle R_n^2 \rangle$ and shown in Fig. 10.

The differential fractal dimension for our longest ($N=1024$) rings in the melt ($\phi=0.5$) is depicted in Fig. 6(a) and compared with their dilute counterparts. The Bragg peak at $r \approx l$ is much more pronounced than for the dilute chains (not fully shown). We again note small, but distinct, σ-dependent packing effects. Not surprisingly, at very large distances the structure is again well described by the Guinier expansion (see Sec. III) and $d_f(q)$ vanishes smoothly.

Obviously one wants to understand the behavior between the (featureless and trivial) Guinier and the (nonuniversal) Bragg part. To stress this regime, in Fig. 6(b) we plot the differential fractal dimension $d_f(q)$ versus $r=2\pi/q$ chopping off distances $r<l$ and the Guinier part. Data are for flexible ($\sigma=0$) and semiflexible ($\sigma=3$) rings and linear chains in the melt. For small distances where $d_f<1$ the data for all d_f are very similar. (Note the small σ-dependent packing effects mentioned above.) At $d_f(r \approx 4)=1$ the semiflexible systems branch off the much steeper line for flexible chains (top line). This also applies to the data for $\sigma=1$ and 2 (not shown). We stress that the difference between different σ is gradual, and that systems of flexible rings do not constitute a singular limit. Because of the small blob size (i.e., the very strong interactions with the surrounding rings) we are unable to separate rigidity and excluded volume effects: Semiflexible rings do not show the ''shoulder'' at $d_f \approx 1$ we saw for dilute rings [the dotted line in Fig. 6(a)].

At these small distances, smaller than the blob size ξ [15], linear chains behave exactly like their ring counterparts of the same flexibility. This proves, as assumed above, that on small scales the σ effects are the same for both architectures, and justifies the use of the persistence length b (and the associated values g_k and k) obtained from linear chains. It also shows that it was natural in Ref. [4] to attempt a finite-size scheme in terms of the correlation hole, at least when one

assumes the CD picture to hold, i.e., R being the only length scale.

However, the rescaling in Fig. 4 did *not* work for molten rings (in contrast to linear chains). This is due to effects caused by the ring closure and topology which intervene at larger distances $r \gg \xi$ (and in particularly at $r \gg d_t$): The fractal dimension d_f for rings continues to rise while the linear chains become roughly Gaussian, i.e., $d_f \approx 2$ [24]. The more flexible the rings, the more this increase becomes suppressed [see the flexible chains of mass $N > 256$ in Fig. 6(b)]. This gives the more rigid systems a chance to catch up [in $d_f(q)$] to the more flexible ones—and this after having consumed fewer monomers on short scales.

The above discussion is only valid if the chains are actually large enough, i.e., $r \ll R_g$ or $S(q) \ll N$, to fall on the asymptotic (σ-dependent) curves. The closure constraint (rather than the topology) forces smaller rings [e.g., $N = 64$ in Fig. 6(b)] to form rather dense globules of blobs.

For (asymptotically) long rings there are now two possible scenarios: Either all the σ lines merge again at large enough distances, or they become parallel. [We reject a crossing of the $d_f(\sigma)$ lines as unphysical.] Unfortunately we are at present unable to decide unambiguously between these two. However, we believe it more likely that all the lines eventually merge and that the asymptotic properties of ring polymers are independent of the persistence length b [25]. Hence, for large distances $r > r^*(\sigma)$, the evolution of $d_f(r)$ again becomes *independent* of σ. It is tempting in view of the scaling in Fig. 9 to set $r^* = d_t$ [26].

G. Local conformational properties: Contour distance R_n

We consider finally the average distance $R_n = \langle (\vec{R}_i - \vec{R}_{i+n})^2 \rangle^{1/2}$ between the ends of a ring contour segment of length n. Similar to the discussion above for $S(q)$, we define a differential fractal dimension $1/d_f = d \log(R_n)/d \log(n)$. Note that $S(q)$ and $\langle R_n^2 \rangle$ are not just simply Fourier transforms of each other. They contain different information: the $S(q = 2\pi/R_n)$ monomers of the reference ring within a volume of radius $\approx R_n$ around an arbitrary monomer of the same ring also comprise monomers far away from the ring contour, i.e., much larger than n. This contribution is certainly small for linear chains [hence $S(q) \propto n$ [12]], but becomes more and more important while the rings become more compact (with increasing σ and N).

We have plotted R_n in the main part of Fig. 10 versus $n \leqslant N/2$ for various ring length masses, as indicated in the figure. Both flexible ($\sigma = 0$) and semiflexible ($\sigma = 3$) are included. The lines of the stiffer rings are stronger curved. For $n \ll N/2$ all curves collapse on a chain length independent (but σ dependent) master curve. Obviously, in the limit of $n \to N/2$ the ring closure forces R_n to level off toward R_e, i.e., $1/d_f$ has to vanish. The inset shows the differential fractal dimension d_f for our longest rings $N = 1024$ for three different persistence lengths. Indeed, d_f for small n increases with σ. For short flexible rings the fractal dimension takes more or less a Gaussian value. Consistent with Fig. 6 we are unable to separate clearly the different length scales, and observe broad crossover lines. As mentioned above, d_f has trivially to diverge for $n \approx N/2$ and data points $n > N/4$ are influenced by this upper cutoff. However, we again see that stiffer chains show more compact scaling than flexible ones. Qualitatively, the $\sigma = 3$ curve is even consistent with the $d_f = 4$ window predicted for Gaussian LA's [7].

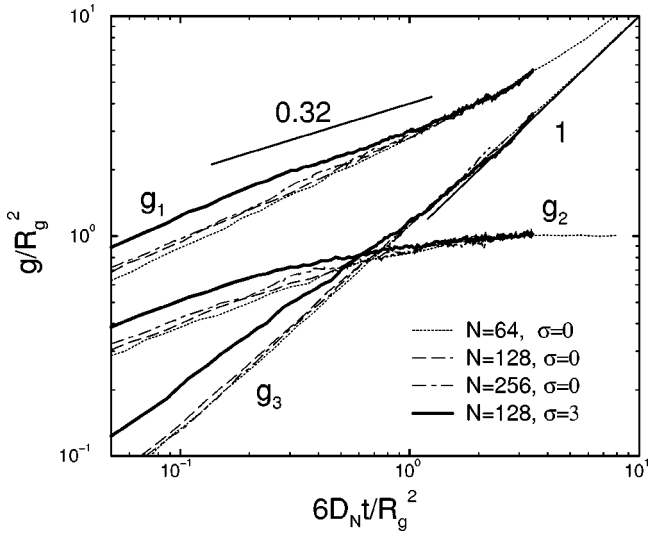

FIG. 11. Reduced mean-square displacements vs reduced time for two rigidities and different chain lengths as indicated in the figure. The scaling works reasonably well for flexible chains ($\sigma = 0$). However, it is inconsistent with the semiflexible ($\sigma = 3$) configurations.

In brief, the advantage to use stiff chains is due to an additional length scale $d_t \propto N^0$. Flexible chains, very compact on short length scales (see the snapshot on the left of Fig. 2), ''waste'' a large number g_t of monomers. Systems with $N \leqslant g_t$ (that is, $R_g \ll d_t$) feature only *one* characteristic size, their own size, and show CD scaling (with $\alpha = 0$). Semiflexible chains, however, using fewer monomers at short distances below d_t, can explore larger distances and become more compact in the scaling sense: They do this by having a lower ceiling on the local density ρ of a single ring, thereby enhancing the topological interaction with their neighbors (thus increasing d_f).

V. DYNAMICS OF RINGS IN THE MELT

The differences in the ring statistics should strongly influence their dynamic behavior. But, as pointed out in Ref. [4], there is some experimental evidence that the dynamics of rings are similar to their linear counterparts, at least up to the largest molecular masses that can readily be obtained. Our simulation data, presented below, confirm this.

We characterize the dynamics by measuring three different mean-square displacement functions describing the motion of monomers $g_1(t) = \langle [\mathbf{R}_n(t) - \mathbf{R}_n(0)]^2 \rangle$ in the laboratory frame, the motion of monomers in the center-of-mass frame of a given ring $g_2(t) = \langle [\mathbf{R}_n(t) - \mathbf{R}_{c.m.}(t) - \mathbf{R}_n(0) + \mathbf{R}_{c.m.}(0)]^2 \rangle$, and the motion of the center of mass itself $g_3(t) = \langle [\mathbf{R}_{c.m.}(t) - \mathbf{R}_{c.m.}(0)]^2 \rangle$. As shown in Fig. 11, the mean square displacements for flexible rings collapse onto chain length independent master curves when the mean square displacements are rescaled by the radius of gyration $\langle R_g^2 \rangle$, and the time by the characteristic relaxation time $\langle R_g^2 \rangle / D_N$. Here D_N is the diffusion coefficient (presented in Fig. 12) obtained from the asymptotic

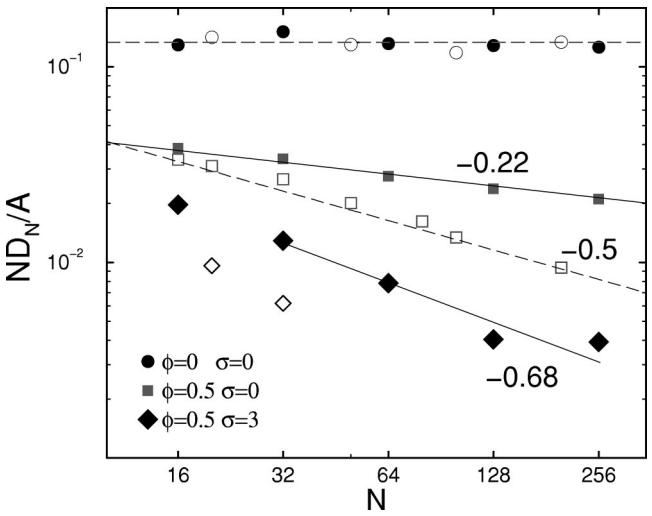

FIG. 12. Diffusion constants ND_N reduced by the acceptance rate A vs N for rings (full symbols) and linear chains (empty symbols). We consider dilute, flexible ($\sigma=0$) chains (circles) and flexible ($\sigma=0$, squares) and semiflexible ($\sigma=3$, diamonds) chains in the melt ($\phi=0.5$). The lines correspond to effective power laws.

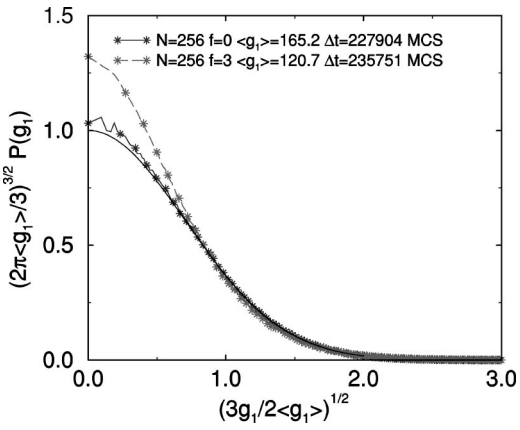

FIG. 13. Probability distribution of mean-square displacements of monomers at short times. Flexible rings ($\phi=0.5,\sigma=0$): Gaussian distribution of monomer displacements at $6D\Delta t/R_g^2=0.42$. Semiflexible rings ($\phi=0.5,\sigma=3$): deviations from the Gaussian behavior at $6D\Delta t/R_g^2=0.02$ indicate an abundance of slow monomers (presumably) within the ''trunk'' of the lattice animal tree. The solid line represents the Gaussian distribution.

behavior of the center of mass motion $g_3(t)/t$ (bold line of slope 1 on the right).

Closer inspection shows, however, that the collapse is not perfect. This is in agreement to what was observed by Brown and Szamel [5]. In any case, this scaling is not born out for the semiflexible ($\sigma=3$) systems of mass $N=128$ depicted in Fig. 11. This does not come as a surprise in view of what we have described above in Sec. IV about the scaling of conformational properties. It is worth noting than in inspection of the differential slope of the motion of monomers $g_1(t)$ (not shown) shows (a small, but distinct) region with slope 0.32 instead of the classical Rouse-like anomalous diffusion exponent $\approx 1/2$.

In Fig. 12 we present the self-diffusion constant of linear chains (empty symbols) and rings as a function of their size N. The circles correspond to isolated swollen chains. The diffusion constant is the same for linear chains and rings. It scales like $D_N \sim 1/N$. Of course our Monte Carlo simulations do not incorporate hydrodynamic interactions, and the dynamics is expected to be Rouse-like [13]. The squares correspond to flexible chains in the melt $\phi=0.5$. It is important to note that rings are always *faster* than their linear counterpart of same mass. As shown in the figure, the diffusion coefficient are well fitted by (effective) power laws: $D_N \propto N^{-1.22}$ for rings and $D_N \propto N^{-1.5}$ for linear chains. As emphasized in Ref. [4], both linear chains and rings scale with the size of their correlation hole $D_N \propto R^{-3}$. The diamonds in Fig. 12 display the results of semi-flexible rings ($\sigma=3$) at melt density $\phi=0.5$. The dependence of the diffusion constant for the larger ring sizes studied is stronger than for flexible chains and obeys the apparent relation $D_N \sim N^{-1.68}$. This is roughly consistent with the data of Brown and Szamel, who found $D \sim N^{-1.54}$ for large flexible rings [5]. Both sets of simulation data are likely to be affected by crossover effects.

This observation is in accord with theoretical calculations, which calculate the diffusion constant of rings via the motion of kinks along the contour. This diffusion of kinks along the molecules is also the dominant relaxation mechanism in the reptation of linear chains. In this sense, the dynamics of (more and more entangled) rings is the analog of reptation in melts of linear molecules. We do not find any signature of arm retraction in the motion of ring polymers. The latter would result in an exponential decrease of the diffusion with ring size like in star polymers [27].

In the (suspected) LA limit, the ring conformations should possess an hierarchical structure. Studying the motion of a single ring in a network of (explicitly) fixed obstacles, Obukov *et al.* suggested that the outer arms of a LA can rearrange much faster than the inner structure [7]. This results in a broad range of relaxation times. We investigated this by monitoring the distribution of mean square displacements of monomers for flexible rings ($N=256$ and $\sigma=0$) and semiflexible ones ($N=256$ and $\sigma=3$) after a time interval $\Delta t \approx 2.3\times 10^5$ Monte Carlo steps. This corresponds to a time scale which is shorter than the diffusion time $D_N/{R_g}^2$ of the ring. Note that both curves (in Fig. 13) correspond to roughly the same time period *and* the same mean value of the monomer displacement. The center of mass diffusion constant differs, however, by an order of magnitude. Hence, the major difference in the dynamic behavior does not stem from a difference in the local dynamics (e.g., a slight decrease of the acceptance ratio of the Monte Carlo moves due to the additional bond angle potential), but reflects the interplay between conformations/topology and the dynamics. Notably, the monomer mean square displacements for flexible rings are Gaussian distributed, while the distribution of semiflexible systems is non-Gaussian. This is consistent with simulations of rings in a network of fixed obstacles [7].

From these different probes of the ring dynamics we conclude that the dynamics for flexible and semiflexible chains are qualitatively different, at least for the chain lengths we were able to probe. There appears to be clear evidence for the occurrence of a second length and time scale for our semiflexible chains (which have $R \geqslant d_t$), but not for our flexible ones (which have $R \leqslant d_t$). Qualitatively we again conclude that stiffer rings are closer to the LA limit than their flexible counterparts. However, even for the largest ring size

and stiffness our data are still affected by the small number of arms, and we expect pronounced finite-size effects to the asymptotic behavior for large rings in the melt. An investigation of the dynamics of even larger rings ($N>256$) is unfortunately beyond our computational facilities at present.

VI. CONCLUSIONS

In summary, we have presented extensive Monte Carlo simulations of semidilute solutions and melts of flexible and semiflexible ring polymers. The rings are neither knotted with themselves nor concatenated with each other.

In order to have a reference with systems where the nonlinkage constraint does not play a role, we have briefly considered dilute solutions of rings. They appear to be extremely similar to their linear counterparts, both with respect to statical and dynamical properties. The (remaining) topological unknottedness constraint seems not to be pertinent [21], at least not for the chain sizes ($N=1024$) we have considered here. The ring extension scales like $R\sim N^{\nu}$ with $\nu\approx 0.59$. This was also made evident from the study of the differential fractal dimension $d_f(q)$ obtained from the static structure factor $S(q)$. Dilute rings do not differ from linear chains with regard to the influence of finite persistence length (at least for large enough rings). The dynamics is Rouse-like $D_N\sim N^{-1}$, because our Monte Carlo simulations ignore hydrodynamical interactions (''free draining limit''). In short, from a practical point of view topology is irrelevant.

This is dramatically different in the high density limit ($\phi=0.5$) with strongly overlapping entangled rings where topological constraints tend to squeeze the rings into relatively compact objects. We have varied the stiffness of the rings so as to tune the overlap between different rings. Due to the rather compact structure of the molecules in the melt, increasing the stiffness is much more efficient than increasing the ring size. Essentially, stiffer chains ''waste'' less monomers on short distances and have more monomers left to meander through the topological constraints imposed by neighboring rings. Indeed the *effective* Flory exponent $\nu(N)$ obtained from the high chain length behavior of chain diameter and radius of gyration shows a strong effect with regard to the persistence length, decreasing from $\nu\approx 0.4$ for flexible chains ($\sigma=0$) to $\nu\approx 1/3$ for our stiffest systems ($\sigma=3$). Chain stiffness allows a reduction in ν to more ''compact'' values by *increasing* (at a given ν) the overlap parameter $p\propto b^3N^{3\nu-1}$.

Rings with topological constraints do not follow the classical one parameter scaling with ϕ/ϕ^* for linear chains where the size of the (dilute) chain of mass N and stiffness σ sets the only relevant length scale [12]. This is in disagreement with the fundamental assumption of the CD picture [6]. In order to scale the chain length $R=R(N,\sigma)$ we were forced to assume an additional chain length independent length scale $d_t\propto g_t{}^{\nu_1}$. Supposing a weak σ dependence of d_t and choosing ν_1 self-consistently, this yields a satisfactory data collapse and $\nu_1\approx 1/2$, as demonstrated in Fig. 9. For small chains, $R\ll d_t$, the topological interactions are weak. The rings resemble their linear counterparts and behave effectively like closed Gaussian chains of blobs. This regime is consistent with the $\alpha\to 0$ limit of the CD scenario, i.e., due to the nonlinkage constraint the free energy of a reference ring increases only like $\log(p)$. Rings larger than d_t appear to be governed by the topological interactions, and are more compact (in the scaling sense of smaller ν). They are well characterized by an effective Flory exponent $\nu_2=1/3$. This scaling scenario is broadly consistent with the concept of *lattice animals* (LA's) within a network of topological obstacles created in a self-consistent manner by surrounding rings [7,9]. These LA's appear to be made of locally Gaussian chain pairs at short distances.

Our (more ambitious) discussion of the differential fractal dimension d_f (obtained from the static structure factor $S(q)$ and/or the spatial distance $R_n(n)$ between a contour segment of length n) reveals very rich and broad crossover effects: excluded volume ξ versus persistence length k, excluded volume versus ring closure, and ring size R versus topological length scale d_t. As shown in Figs. 6 and 10, it is not possible to separate the different length scales unambiguously and to disentangle their physics [28]. In view of the (restricted) range of parameters ($N\leqslant 1024, \sigma\leqslant 3, \phi=0.5$) we are able to simulate, this does not come as a surprise. Much more surprising is the success and the simplicity of the scaling scenario of Fig. 9 for the global chain R size described in the paragraph above. There, all the intricate short range physics was cast in *one* effective exponent ν_1 for all chain and persistence lengths. It just turns out that the Gaussian value $\nu_1=1/2$ (i.e., $\alpha\to 0$) fits the data particularly well. Similarly, while $\nu_2=1/3$ is certainly the asymptotic value, this does not exclude the possibility of a large intermediate window with $\nu_2=1/4$ [7,29]. Indeed the differential fractal dimensions for our largest and stiffest configurations clearly exceed $d_f=3$. This is in favor of an ultracompact transient, which should then eventually also become evident in the ring sizes for even larger chain lengths N than we are at present able to simulate.

Additional evidence for the crossover to a strongly entangled regime characterized by an additional length scale d_t comes from our brief investigation of the ring dynamics. The scaled time dependence of the monomer displacements differs from the master curve in the non-entangled regime, and the monomer displacements at times smaller than the relaxation time are non-Gaussian distributed, as expected for LA's [7]. The diffusion constant for chains in the melt scales like $D_N\sim N^{-1.22}$ for flexible chains. This decrease to $D_N\sim N^{-1.68}$ for semiflexible systems ($\sigma=3$). Again these exponents are presumably only effective values due to a broad crossover between unentangled and entangled regimes. The similarity of the dynamics of melts of rings and linear chains suggests that our observations for rings might also be pertinent to the dynamics of linear chains. Indeed, it is tempting to relate the topological constraints which lead to the lattice animal behavior for rings to the entanglements in linear chains. While the topological interactions do not influence the static conformations of linear chains, however, rings offer the additional possibility to investigate the effect of topology in the static behavior.

In any case, our simulation data cover only the onset of LA behavior and our estimates for the scaling functions of the conformational statistics and the dynamics are likely to be subjected to corrections due to the very small number of arms. In the future we plan to corroborate further the discussion of the dynamical properties (increasing the number of

statistical segments) and to investigate the static and dynamical scaling properties with regard to the monomer density ϕ [14].

ACKNOWLEDGMENTS

M.M. benefitted from interesting discussions with W. Paul, K. Binder, and K.S. Schweizer. He thanks E.P.C.C. for very kind hospitality and financial support during his stay as a TRACS visitor and J.-C. Desplat for visualizations of the ring conformations (Fig. 2). A generous grant of CPU time on the Cray T3E computers at the EPCC in Edinburgh and the HLR Stuttgart as well as partial financial support by the DFG under Grant Bi314-17 are gratefully acknowledged. J.P.W. acknowledges stimulating discussions with S.P. Obukov that triggered this study. Finally he would like to thank C. Gay and J.-L. Barrat for detailed comments concerning the topological constraints.

[1] Unknotted and unconcatenated ring polymers have actually been made and investigated experimentally. In Ref. [4] the reader will find a detailed account of results and technical difficulties related to ring synthesis and contamination with linear rings. We do not wish to repeat this here. (Also see Ref. [2].) All these studies focus on dynamical properties. No experimental study of the radius of gyration of rings in melt appears to have been made until now—despite the fact that any reasonable description of dynamics requires a good understanding of conformational properties.

[2] T. P. Lodge, N. A. Rotstein, and S. Prager, Adv. Chem. Phys. **79**, 1 (1990).

[3] T. Pakula and S. Geyler, Macromolecules **21**, 1665 (1988).

[4] M. Müller, J. P. Wittmer, and M. E. Cates, Phys. Rev. E **53**, 5063 (1996).

[5] S. Brown and G. Szamel, J. Chem. Phys. **109**, 6184 (1998).

[6] M. E. Cates and J. M. Deutsch, J. Phys. (France) **47**, 2121 (1986).

[7] S. P. Obukhov, M. Rubinstein, and T. Duke, Phys. Rev. Lett. **73**, 1263 (1994).

[8] M. G. Brereton and T. A. Vilgis, J. Phys. A **28**, 1149 (1995).

[9] A. R. Khokhlov and S. K. Nechaev, Phys. Lett. A **112**, 156 (1985); J. Phys. II **6**, 1547 (1996).

[10] Note that ring closure is a *necessary* condition for the topological constraints we are focusing on. It is a relatively simple matter to conceive an algorithm for closed chains which violate topology. Hence closure and topology constraints are related, but distinct, properties.

[11] M. D. Frank-Kamenetskii, A. V. Lukashin, and A. V. Vologodskii, Nature (London) **258**, 398 (1975).

[12] P.-G. de Gennes, *Scaling Concepts in Polymer Physics* (Cornell University Press, Ithaca, NY, 1979).

[13] M. Doi and S. F. Edwards, *The Theory of Polymer Dynamics* (Clarendon Press, Oxford, 1986).

[14] M. Müller, J. P. Wittmer, and M. E. Cates (unpublished).

[15] W. Paul, K. Binder, D. Heermann, and K. Kremer, J. Phys. II **1**, 37 (1991); J. Chem. Phys. **95**, 7726 (1991).

[16] J. Wittmer, W. Paul, and K. Binder, Macromolecules **25**, 7211 (1992).

[17] H.-P. Deutsch and K. Binder, J. Chem. Phys. **94**, 2294 (1991); I. Carmesin and K. Kremer, Macromolecules **21**, 2819 (1988).

[18] M. Müller, EPFL Supercomput. Rev. **7**, 21 (1995).

[19] M. Müller, Macromolecules **28**, 6556 (1995); M. Müller and A. Werner, J. Chem. Phys. **107**, 10 764 (1997).

[20] These estimates depend strongly on the further evolution of the effective Flory exponent $\nu(N)$ discussed below. However, the balance remains strongly favorable even if the computational overhead (to calculate the additional potential), the reduced acceptance rate A (see Table II), and (more importantly) the slower diffusion (see Fig. 12) are taken into account.

[21] Recently the effects of non-self-knotting for dilute rings with extremely weak excluded volume interactions were investigated by J. M. Deutsch, Phys. Rev. E **59**, R2539 (1999). His Monte Carlo simulations indicate surprisingly that the extension of these chains still scale with the same exponent $\nu \approx 3/5$ due to the unknottedness constraint.

[22] We have also tried values based on the effective bond lengths for Gaussian chains from Ref. [16] quoted in Table II. However, the results are virtually identical.

[23] Let us assume that the ring consists of uncorrelated needlelike arms of a fixed length Δ. Two segments on the same arm are either parallel or antiparallel; the directions of different arms are completely uncorrelated. For this crude model the bond-bond correlation function $\langle \vec{e}_i \vec{e}_{i+n} \rangle$ decays linearly from 1 at $n=0$ to $-1/2$ at $n=\Delta$, and then increases linearly to 0 at $n=2\Delta$. For larger distances n along the chains there are no correlations by construction. This motivates the assumption that a minimum in the bond-bond correlation function is associated with a backfolding, and the position of the minimum is an estimate of the arm length. Certainly, there is a distribution of arm lengths, and the correlation along an arm is not perfect. This will broaden the minimum. More important, the above argument neglects the hierarchical structure of lattice animals and only captures local correlations.

[24] Note that even for linear chains of length $N=256$ we do not obtain a perfect Gaussian plateau, but rather a flattish hump [see Fig. 6(b)]. This provides an important warning. Even for the linear chains it is tricky to reach the asymptotic limit for the differential fractal dimension.

[25] Admittingly *a priori* it is not excluded that b triggers a continuous spectrum of universality classes.

[26] Accepting that all lines will merge eventually, we have to ask how they will do so. The simplest suggestion is that they all merge together at one point r^*. Then no persistence length, e.g., the $d_f(\sigma=0)$ line, is singled out. Otherwise one may characterize each persistence length by the point $r^*(\sigma)$ where it joins the flexible ring line $d_f(\sigma=0)$.

[27] J. Klein, Macromolecules **19**, 105 (1986).

[28] Not to mention logarithmic corrections due to weak topological interactions in the $\alpha \to 0$ limit of the CD regime.

[29] It was estimated in S. P. Obukhov, M. Rubinstein, and R. H. Colby, Macromolecules **27**, 3191 (1994) that the $d_f=4$ regime could last until $N=30\,000$.